Environ Geochem Health (2024) 46:60
https://doi.org/10.1007/s10653-024-01858-y

ORIGINAL PAPER

# Identifying sources of acid mine drainage and major hydrogeochemical processes in abandoned mine adits (Southeast Shaanxi, China)

**Wentong Chang · Xianmin Ke · Wei Wang · Peng Liu**

Received: 28 June 2023 / Accepted: 3 January 2024 / Published online: 27 January 2024


**Abstract** Acid mine drainage (AMD) has resulted in significant risks to both human health and the environment of the Han River watershed. In this study, water and sediment samples from typical mine adits were selected to investigate the hydrogeochemical characteristics and assess the environmental impacts of AMD. The interactions between coexisting chemical factors, geochemical processes in the mine adit, and the causes of AMD formation are discussed based on statistical analysis, mineralogical analysis, and geochemical modeling. The results showed that the hydrochemical types of AMD consisted of $SO_4$–Ca–Mg, $SO_4$–Ca, and $SO_4$–Mg, with low pH and extremely high concentrations of Fe and $SO_4^{2-}$. The release behaviors of most heavy metals are controlled by the oxidation of sulfide minerals (mainly pyrite) and the dissolution/precipitation of secondary minerals. Along the AMD pathway in the adit, the species of Fe-hydroxy secondary minerals tend to initially increase and later decrease. The inverse model results indicated that (1) oxidative dissolution of sulfide minerals, (2) interconversion of Fe-hydroxy secondary minerals, (3) precipitation of gypsum, and (4) neutralization by calcite are the main geochemical reactions in the adit, and chlorite might be the major neutralizing mineral of AMD with calcite. Furthermore, there were two sources of AMD in abandoned mine adits: oxidation of pyrite within the adits and infiltration of AMD from the overlying waste rock dumps. The findings can provide deeper insight into hydrogeochemical processes and the formation of AMD contamination produced in abandoned mine adits under similar mining and hydrogeological conditions.

**Keywords** Acid mine drainage · Pyrite · Hydrogeochemistry · Abandoned mine · PHREEQC

## Introduction

The exploitation of mineral resources results in a great number of tailings and waste rock dumps, which is one of the most hazardous types of solid waste. Acid mine drainage (AMD) is the most concern among the environmental pollution caused by tailings and waste rock piles (Acharya & Kharel, 2020; Akcil & Koldas, 2006; Servida et al., 2009). Moreover, AMD is one of the severe environmental problems due to its serious hazards, large scale of pollution, and highly difficult remediation process (Hermassi et al.,

**Supplementary Information** The online version contains supplementary material available at https://doi.org/10.1007/s10653-024-01858-y.

W. Chang · X. Ke · W. Wang (✉) · P. Liu
School of Water and Environment, Chang'an University, Xi'an 710054, Shaanxi, China
e-mail: wangweichd@chd.edu.cn

W. Chang · X. Ke · W. Wang · P. Liu
Key Laboratory of Subsurface Hydrology and Ecological Effect in Arid Region of the Ministry of Education, Chang'an University, Xi'an 710054, Shaanxi, China

2022; Naidu et al., 2019), and it is prevalent in countries with large pyrite reserves, such as Spain, China, and the USA (Sánchez España et al., 2005; Tu et al., 2022; Zhao et al., 2012). Currently, AMD research not only focuses on hydrogeochemical processes in the AMD environment but also the innovation of pollution remediation techniques. More new techniques and AMD sludge composites were used to adsorb and recover sulfuric acid and heavy metals from AMD (López et al., 2019; Zhang et al., 2022). Compared to the subsequent remediation of AMD, it will be fundamentally important to study the formation of AMD and develop effective measures, to prevent their formation during the mining process, and ultimately to address the worldwide challenge of AMD pollution (Xiying et al., 2020).

AMD is an acidic (typical pH range of 2.5–5), heavy metal-rich wastewater produced by the oxidation of sulfide minerals (mainly pyrite) in abandoned mines. Sulfide minerals are stable and insoluble under reductive conditions. Consequently, pyrite and other sulfides are preserved in anoxic environments, preventing the mobilization of heavy metals and acids. However, when the reactive mineral comes into contact with oxygen and atmospheric moisture, the oxidation process of sulfide minerals occurs (Sáinz et al., 2003). The AMD not only degrades water quality by flowing into groundwater, rivers, and streams, but also results in the contamination of sediments, causing numerous environmental problems. Thus, even when the river and creek become clean during non-acidic periods or after AMD treatment, sediments containing heavy metals are still a potential environmental threat to humans and wildlife. AMD sediments are one of the contributing factors to heavy metal contamination of soil, and crops can absorb heavy metals from contaminated soil, which may harm human health through the food chain (Caraballo et al., 2011; Simate & Ndlovu, 2014).

In the water–sediment system, different chemical conditions (e.g., pH and the valence state of Fe) formed different combinations of Fe-containing secondary minerals, and the adsorption, co-precipitation, and transformation across the water–sediment interface led to the differences in heavy metal distribution (Li et al., 2014; Qian et al., 2019). Fe secondary minerals (e.g., goethite, jarosite, and schwertmannite) adsorb and coprecipitate heavy metals and store acidity in the AMD environment, which is essential for attenuating heavy metals in AMD (Chen et al., 2020). However, the secondary minerals transform or dissolve to release the stored acidity and heavy metals when the chemical conditions change, resulting in secondary contamination. The mineralogy of AMD sediments is important not only for establishing the hydrogeochemistry of the AMD but also for AMD treatment.

Some scholars have carried out studies on AMD hydrogeochemical characteristics because of its hazards, using statistical methods such as correlation analysis and cluster analysis to identify the sources of heavy metals in contaminated water under the influence of natural processes or human activities (Moreno-González et al., 2022; Xiying et al., 2020). Most of their research has focused on AMD formed in open pits or waste rock piles, and the attenuation process of AMD flowing into rivers and streams. However, the formation of AMD pollution within mine adits is ignored (Liu et al., 2023; Newman et al., 2023). The mine adit is a perpetual pollution machine, with various hydrogeochemical processes occurring at different distances based on hydrogeochemical conditions and microbial environments. The AMD formed in the mine adit is the most contaminated and contributes the majority of water pollution downstream (Han et al., 2017; Kotalik et al., 2021; Tomiyama et al., 2020). The remediation of the abandoned mine adits should be emphasized because of its extreme hazards and serious environmental impacts (Kim et al., 2023). In certain areas of China, pyrite was primarily extracted through the mine adits, resulting in multiple intermittent point sources of AMD pollution in the mining area (Wu et al., 2006; Yue et al., 2006). AMD accumulated in mine adits before the rain and was subsequently discharged after the rain, continually contaminating the water environment in the watershed. Hence, understanding the hydrogeochemical processes occurring in mine adits is highly important because of the influence that they exert on the heavy metals and acids transported to groundwater, rivers, and streams.

In the 1970s, large-scale pyrite mining in Baihe County (Southeast Shaanxi, China) was conducted. Due to the old mining technology and the lack of awareness of environmental protection, the mine adits were abandoned after pyrite mining, and a large amount of waste rock was piled up and scattered. With time, a large amount of AMD was accumulated

in the abandoned mines due to atmospheric oxidation and rainwater leaching, which was discharged directly into the nearby rivers, causing the degradation of river water quality. This increased surface water pollution and the destruction of the aquatic ecosystem in mining areas seriously affect the livelihood of residents and the Han River's water quality. The Han River, one of China's most valuable rivers, is the largest tributary of the Yangtze River and the water source of the Middle Route of China's South to North Water Transfer Project (Li & Zhang, 2010; Li et al., 2009). It also provides significant biological and hydropower resources. However, no research has been conducted in the Baihe mine area to understand the hydrogeochemical information in various pollution factors of AMD. With the treatment of AMD to be carried out in the next two years, it is necessary to investigate and analyze the hydrogeochemistry of AMD in the mine adit, so that proper treatment strategies can be developed according to the contamination conditions and characteristics.

In this study, we analyzed the composition of the liquid and sediment phases in AMD from the Baihe mine. Moreover, the interactions between the chemical components, focusing on the presence of the contaminants (including heavy metals, metalloids, $SO_4^{2-}$, inorganic nitrogen (N), and other pollution indicators that contribute to the hazards of AMD) and the correlation between them, were also studied. The present study aims to (1) establish the database on hydrogeochemistry of AMD in mine adit; (2) identify the key factors influencing the evolution of AMD contamination; (3) assess the degree of AMD contamination using acid mine drainage index (AMDI); (4) identify the major hydrogeochemical processes inside the adit by combining geochemical modeling and hydrogeochemical analysis; and (5) clarify the special source of AMD in the mine adit. This will provide a reliable basis for the improvement and remediation of the mine environment affected by AMD.

## Materials and methods

### Overview of the study area

The study area is located southeast of Baihe County, Shaanxi Province, and east of Daba Mountain. Several pyrite deposits have been discovered in the southern part of Shaanxi Province due to the extensive geological work carried out in China in the last century. This study focuses on four abandoned mine sites, DBS, TLG, JCG, and LHC, in the Xiba and Dongba River area (Fig. 1). The climate of the study area is humid continental monsoon (mild climate) with mean annual precipitation of 500–800 mm (the main precipitation period being from April to October). The surface water system in the area is based on the Xiba and Dongba River system, belonging to the Baishi River system (the length is 88.5 km, and a catchment area is 807 $km^2$, covering 55.7% of the total area of Baihe County), which originates from Jieling and ends in the Han River (flows from south to north). The Baishi River receives surface drainage from the four abandoned mine sites that originate from waste rock dumps and mine adits. According to the survey report, the total drainage flow rate of these mine sites ranges from 1061.94 to 2727.91 $m^3/d$, making them significant contributors to the Baishi River. The total length of the impacted water body and riverbed, which are yellowish brown and muddy, is more than 55 km.

The study area mostly consists of low–medium mountains (altitude ranging from 1000 to 2000 m) with steep hills and deeply incised valleys, providing suitable drainage conditions for discharging AMD from abandoned mines into the downstream residential areas. The Baihe pyrite ore deposit is controlled by the hydrothermal alteration of volcaniclastics, formed within green tuff host rock. Pyrite ore bodies comprise pyrite as the main mineral composition and pyrrhotite, chalcopyrite and sulfur in small amounts, and the ore minerals exhibit banded, nodular, and disseminated textures. The aquifers in the region can be classified into three types based on their occurrence conditions, physical properties, and hydrological characteristics: (1) loose pore water of the Quaternary system (comprising mainly of fine silt and gravelly soil); (2) pore water of the waste rock layer (comprising mainly of crushed and block stone from the waste rock); and (3) fissure water in bedrock (comprising mainly of tuff, spilite and carbonaceous schist). Groundwater in the study area is mainly recharged by precipitation. In the mine adit, groundwater seeps out of the surrounding rock fissures and forms the pit water, which then flows over or through the bottom floor before being discharged into streams or seeping into

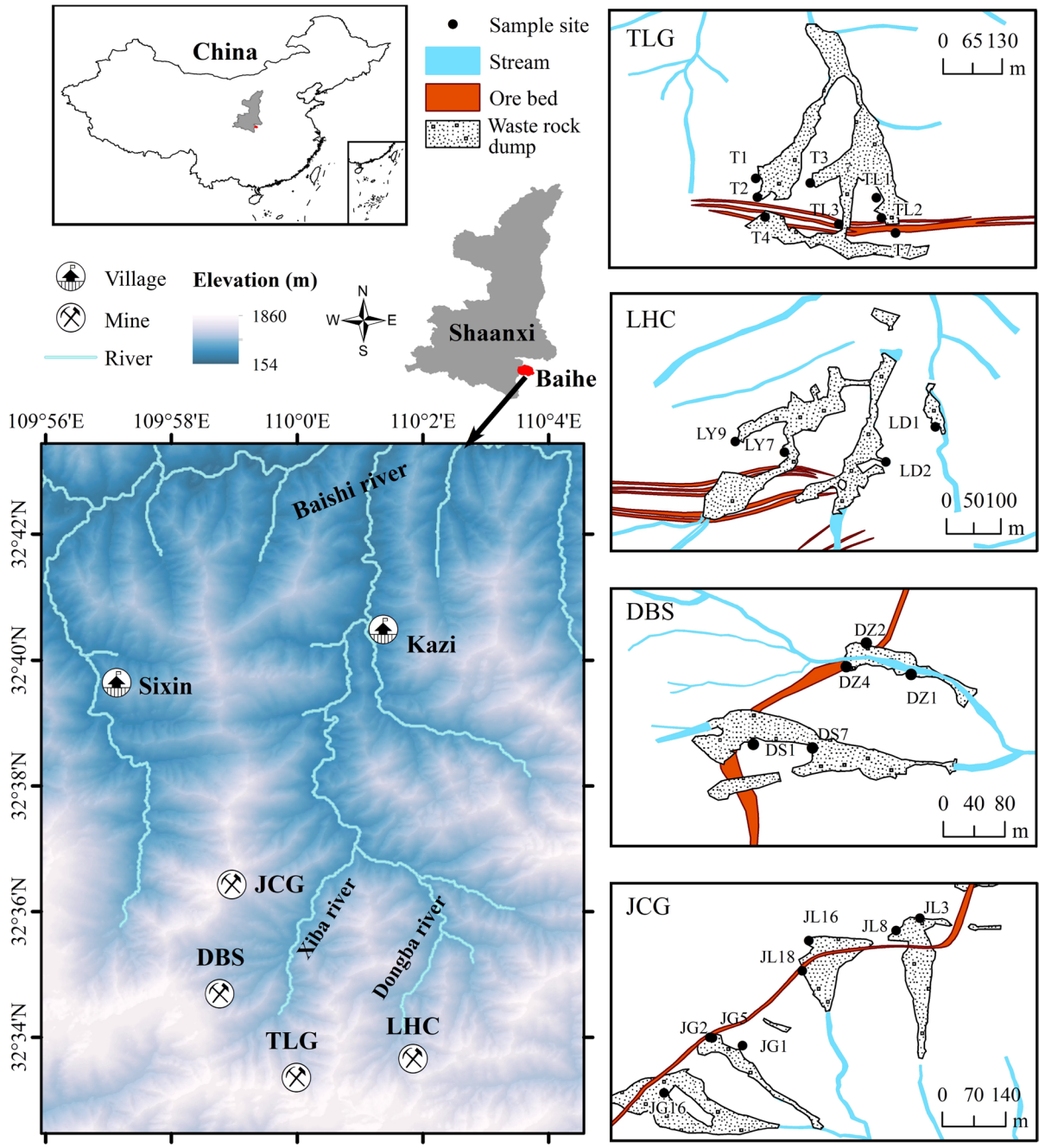


**Fig. 1** Map of study area showing the location of sampling sites (water samples were collected at all sampling sites, and sediment samples were collected at adit J16)

the waste rock dumps outside of the adit. Groundwater in this area is characterized by short runoff paths, active water exchange and weak dissolution due to the topography, lithology, and tectonics.

## Sampling

Water samples from typical mine adits were collected from March to May 2022 mostly at the entrance (25

sampling sites) and also at particular positions (9 sampling sites including adit branch confluence, pyrite deposit, and seepage cracks) in the adit, with 25 of these sites being collected before and after rainfall to study the influence of precipitation. Post-rainfall sampling was started at least two days after the rain ended to include the lagged effects of recharge of fissure water (groundwater circulating in the fissure of host rocks or altered rocks) by precipitation infiltration. A total of 59 sets of water samples were collected using a water sampler at every sampling site, allowed to settle for five minutes, filtered through a 0.45-μm acetate membrane, and then stored in fully rinsed polyethylene plastic containers. Water samples for trace metal content assays were acidified with concentrated nitric acid to a pH of about 2, and all examples were kept at roughly 4 degrees Celsius before detection.

A total of 6 sets of sediment samples were collected at 3 m, 23 m, 43 m, 58 m, 74 m, and 84 m from the entrance of the typical mining adit J16 using a fully rinsed plastic shovel sampler, packed in a zip lock bag and stored in the icebox, returned to the laboratory as soon as possible, and then placed in a shaded area of the laboratory to dry naturally. Next, the sediment samples were prepared for X-ray diffraction (XRD) by picking out stones and grinding them in a mortar to a grain size of less than 74 μm.

## Analysis method

Major cations ($K^+$, $Na^+$, $Ca^{2+}$, $Mg^{2+}$and $NH_4^+$), major anions ($Cl^-$, $HCO_3^-$, $CO_3^{2-}$and $SO_4^{2-}$), trace elements (Fe, Mn, Cu, Pb, Cd, Zn, Se and As), and wastewater indicators including pH, redox potential (Eh), total hardness (TH), chemical oxygen demand ($COD_{Cr}$), ammonia nitrogen ($NH_3$-N), and total dissolved solids (TDS) in the water samples were all measured as the indicators of AMD. The pH and Eh were measured in the field using a portable meter (Jenco 6250 pH/mV/ION Meter, China), and the locations of the sampling site and seepage in the mine adit were recorded. The analysis of water samples was carried out at Shaanxi Engineering Survey and Design Institute: pH was also measured by a precision pH meter (pHS-3C); $K^+$, $Na^+$, $Ca^{2+}$, $Mg^{2+}$, Fe, Mn, Cu, Pb, Cd, and Zn were measured by atomic absorption spectrophotometer (AA-7002A); $NH_3$-N and $NH_4^+$ were measured by ultraviolet–visible spectrophotometer (UV-1800); $HCO_3^-$ and $CO_3^{2-}$ were measured by acid–base titration; $Cl^-$ was determined using silver nitrate titration; $SO_4^{2-}$ was determined using $Na_2$EDTA–Ba titration; $COD_{Cr}$ was determined using dichromate titration; TH was determined using the EDTA titration; Se and As were measured by a double-channel atomic fluorescence photometer (AFS-2202E); and TDS was measured by weighing method using BSA124S electronic scale. During the testing process, quality control is carried out for all indicators by using certified reference materials provided by the National Standards Center or spike-and-recovery assessment. To ensure the accuracy of the measurements, each sample was divided into two samples, and the average value of the two samples was considered within the error tolerance. The test results of all certified reference materials are required to fall within confidence intervals, with the percent recoveries of elements between 90 and 110% and an uncertainty of ± 20% for percent recoveries.

The XRD analysis provides information on the internal structure, morphology, and other phase structure of the sediment by diffraction peak pattern. The XRD analysis was carried out with an X-ray diffractometer (Ultima IV, RIGAKU, Japan) under the following conditions: Cu Kα X-ray source (40 kV, 30 mA), 0.02° step-scan mode, and $2\theta$ range of 5–90°. Pattern interpretation was performed using MDI Jade 6 and combined with powder diffraction file (PDF) -2004 cards. Due to field sampling and the strong fluorescence effect caused by Fe and Mn elements, the diffraction peak patterns were properly smoothed, and the background was removed (Yang et al., 2021).

Assessing the contamination degree of the affected groundwater and surface water is difficult by individual chemical indicators, so some scholars have proposed an objective evaluation index, the acid mine drainage index (AMDI). AMDI is calculated using a modified arithmetic weighted index of the most indicative pollution factors (pH, $SO_4^{2-}$, Fe, Zn, Al, Cu, Cd, a total of seven parameters) to quantify AMD pollution. The acid mine drainage index (AMDI) was used to evaluate the degree of water pollution in the study area, and the AMDI value was calculated by Gray's equation (Eq. (1)) using the water quality ratings for each parameter in Table 1 (Gray, 1996); generally the lower the score, the more serious the contamination. Because of the less development of aluminum-bearing surrounding rocks in the study area, the preliminary experiments did

**Table 1** Water quality ratings for acid mine drainage and contaminated surface water and groundwater

| Score | pH | $SO_4^{2-}$(mg/L) | Fe(mg/L) | Zn(mg/L) | Cu(mg/L) | Cd(μg/L) |
|---|---|---|---|---|---|---|
| 25 | | < 10 | | | | |
| 24 | | 10–14 | | | | |
| 23 | | 15–29 | | | | |
| 22 | | 30–49 | | | | |
| 21 | | 50–99 | | | | |
| 20 | > 6.5 | 100–199 | | | | |
| 19 | 6.2–6.4 | 200–299 | | | | |
| 18 | 5.9–6.1 | 300–399 | | | | |
| 17 | 5.6–5.8 | 400–499 | | | | |
| 16 | 5.2–5.5 | 500–599 | | | | |
| 15 | 4.9–5.1 | 600–799 | < 0.05 | | | |
| 14 | 4.5–4.8 | 800–999 | 0.05–0.99 | | | |
| 13 | 4.1–4.4 | 1000–1499 | 1.00–4.99 | | | |
| 12 | 3.9–4.0 | 1500–1999 | 5.00–9.99 | < 0.05 | | |
| 11 | 3.7–3.8 | 2000–3999 | 10–24 | 0.05–0.49 | | |
| 10 | 3.5–3.6 | 4000–5999 | 25–49 | 0.5–0.9 | | < 10 |
| 9 | 3.3–3.4 | 6000–7999 | 50–99 | 1.0–4.9 | | 10–24 |
| 8 | 3.1–3.2 | 8000–9999 | 100–149 | 5.0–9.9 | < 0.05 | 25–49 |
| 7 | 2.9–3.0 | 10,000–11999 | 150–199 | 10–24 | 0.05–0.99 | 50–99 |
| 6 | 2.7–2.8 | 12,000–13999 | 200–249 | 25–49 | 1.0–4.9 | 100–249 |
| 5 | 2.5–2.6 | 14,000–15999 | 250–499 | 50–74 | 5.0–9.9 | 250–499 |
| 4 | 2.3–2.4 | 16,000–17999 | 500–749 | 75–99 | 10–24 | 500–749 |
| 3 | 2.1–2.2 | 18,000–19999 | 750–999 | 100–249 | 25–49 | 750–999 |
| 2 | 1.8–2.0 | 20,000–21999 | 1000–1999 | 250–499 | 50–99 | 1000–1499 |
| 1 | 1.5–1.7 | 22,000–24999 | 2000–2999 | 500–749 | 100–249 | 1500–1999 |
| 0 | < 1.4 | > 25,000 | > 3000 | > 750 | > 250 | > 2000 |

not detect the aluminum in the water samples, the Al score was not accounted for the AMDI score, and the AMDI calculation equation was optimized (Eq. (2)).

The Pearson correlation coefficient (the correlation value ($r$) varies from + 1 to –1) and hierarchical clustering (based on Ward's method) between contaminants were used to determine the relationships between the indicators in AMD (Santisteban et al., 2022). Microsoft Excel 2019, SPSS 26, and Origin 2022 were used for data processing, statistical analysis, and graphic drawing in this study.

$$\mathrm{AMDI} = \left[\sum (\text{water quality scores})\right]^2 / 100 \quad (1)$$

$$\mathrm{AMDI} = \left[\sum (\text{water quality scores}) \times \left(\frac{1}{0.9}\right)\right]^2 / 100 \quad (2)$$

## Geochemical modeling

The presence and proportion of dissolved components in AMD were simulated using Phreeqc Interactive 3.7.3 geochemical modeling software (Hu et al., 2021; Schmidt et al., 2020), and WATEQF.dat, a database commonly used to solve AMD problems (Ball & Nordstrom, 1991).

The SOLUTION module of PHREEQC is used to calculate the mineral phases and saturation indices (SI) formed by the samples, which can be used to determine the dissolution/precipitation state of each mineral, especially the dissolution of minerals (Chidambaram et al., 2012). The input data were based on reasonable assumptions from field investigations. The temperature was maintained at 25 degrees Celsius, and the equilibrium constants of minerals such as jarosite, ferrihydrite, and goethite were calculated according to the thermodynamic database

WATEQ4F. The solubility product value (log $K_{sp}$) for schwertmannite based on field observations or laboratory experiments values has been observed to range from 5.8 to 39.5 (Schoepfer & Burton, 2021). In this study, the solubility product value of schwertmannite was determined to be log $K_{sp} = 18.00 \pm 2.50$, using data from Bigham as a reference due to its consistency with the XRD analysis and in situ measurement. (Bigham et al., 1996b). Based on the calculation results, a preliminary determination of the phases of secondary minerals produced in the sediments can be made.

Using the INVERSE MODELING module of PHREEQC, the molarity of dissolved or precipitated minerals was calculated by setting the initial and final water quality data and the mineral phases that may be involved in the reaction (Parkhurst & Appelo, 1999). Positive mole transfer values indicate the dissolution of minerals and negative values indicate precipitation. The results of the inverse simulation can be used to infer geochemical reactions and explain the differences in composition between the initial and final water sources. Four assumptions are required to be satisfied for the inverse simulation: (1) the two water analyses are from the initial and final for water flowing along the same flow path, (2) dispersion does not significantly affect the water chemistry, (3) chemical stability is prevalent in the water system during the time considered, and (4) the mineral phases used for the inverse calculation are or were present in the aquifer (Sharif et al., 2008).

## Results and discussion

### Hydrochemical characteristics

The results of the water samples from the four mine sites are shown in Table S1 and Table S2.

The water quality of the four mine sites was compared using box and whiskers plots (Fig. 2), using a range of ± 1.5 interquartile range for the outliers. The most serious contamination was found at TLG, and pH, Fe, $SO_4^{2-}$, Mn, As, and Cu concentrations were

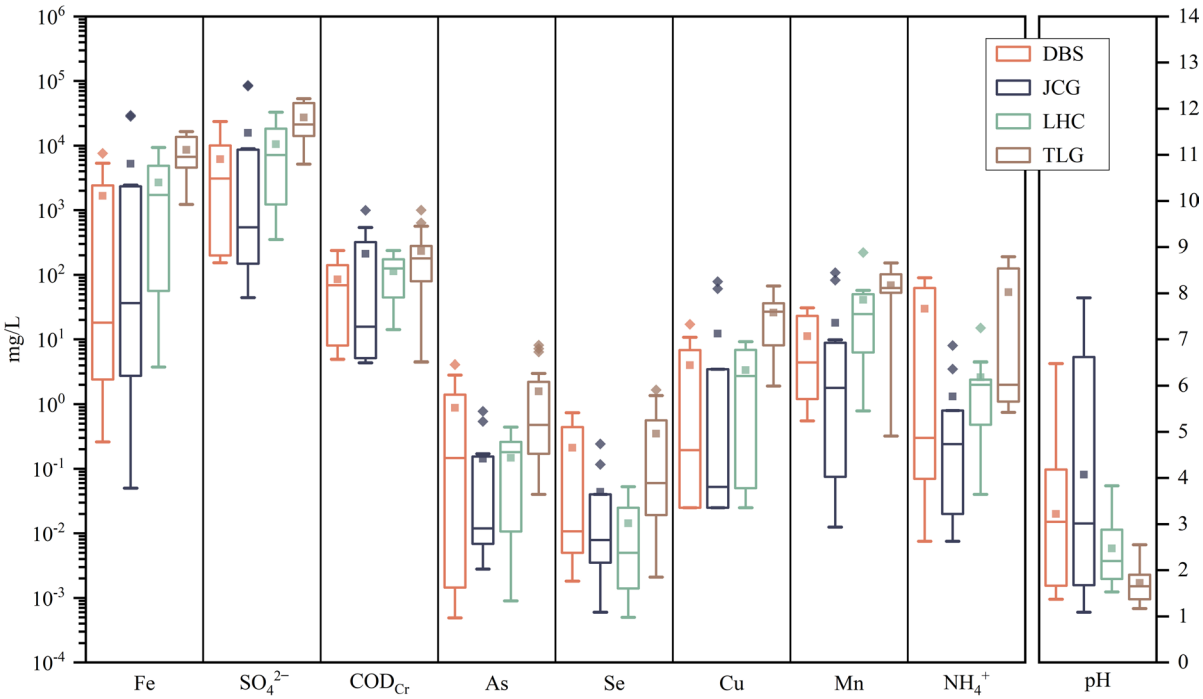


**Fig. 2** Box and whiskers plot for AMD main contamination factor ($n = 12$ for DBS, $n = 12$ for JCG, $n = 13$ for LHC, and $n = 22$ for TLG). The height of each box represents the interquartile range containing 50% of values, the horizontal line inside the box shows the median value, and the square indicates the mean value. The whiskers are lines that extend from the box to the highest and lowest values excluding outliers (Rhombus)

considerably higher than background values (uncontaminated spring) after rainfall. This is because of the partial collapse of channels between most of the chambers and the pits in TLG, resulting in not only a large amount of residual pyrite ore bodies but also waste rock dumps in the adits, providing more adequate conditions to form AMD. Abnormal values for the main contaminants in JCG are mainly attributed to the high elevation of some of the mine entrances. Consequently, a high accumulation of AMD at the entrance and the prolonged retention of contaminants in the standing water make the contamination levels much higher in this adit than those found at other mine sites.

According to the preliminary survey, the background water quality and chemistry for uncontaminated surface water and spring are normal. The water was acidified after leaching and oxidation at the waste rock dump and mine adit; the water in the mine adit showed low pH, high concentration of TDS, and extremely high Fe and $SO_4^{2-}$ concentrations, while $COD_{Cr}$, Mn, Cu Zn, As, and Se were also higher than background values. From the Piper diagram (Fig. 3), it is apparent that most of the hydrochemical types of mine adit water are $SO_4$–Ca·Mg, $SO_4$–Ca and $SO_4$–Mg (the DBS and JCG are mainly $SO_4$–Ca·Mg, while the TLG and LHC are mainly $SO_4$–Mg), which are heavily polluted with $SO_4^{2-}$, with little change in hydrochemical types before and after rain.

The high Fe and $SO_4^{2-}$ concentrations in the AMD were caused mainly by the oxidation of pyrite, with Fe and $SO_4^{2-}$ dominating the anions and cations, respectively, even with concentrations of 28.4 g/L and 85.6 g/L at 35 m in the JG2 chamber. Also, Fe and $SO_4^{2-}$ were the main contributors to TDS in AMD, resulting in abnormally high TDS values. The high concentrations of trace elements such as Mn, Cu, Zn, and As were mainly attributed to three factors: (1) trace elements in the coal-bearing strata in the form of sulfides, oxides, and carbonates were released by dissolution in contact with the strong acidic AMD; (2) trace elements were present in the pyrite through a homogeneous form and released simultaneously during their oxidation (McGregor et al., 1998); (3) heavy metal ions did not easily precipitate with hydroxides, mostly in the ionic form present in water, in an acidic environment. According to the carbonate balance, carbonates were mostly present as $H_2CO_3$ or free $CO_2$ in a low pH environment, which led to the general absence of $HCO_3^-$ and $CO_3^{2-}$ in AMD. Moreover, the dissolution of calcite and dolomite resulted in high concentrations of Ca and Mg.

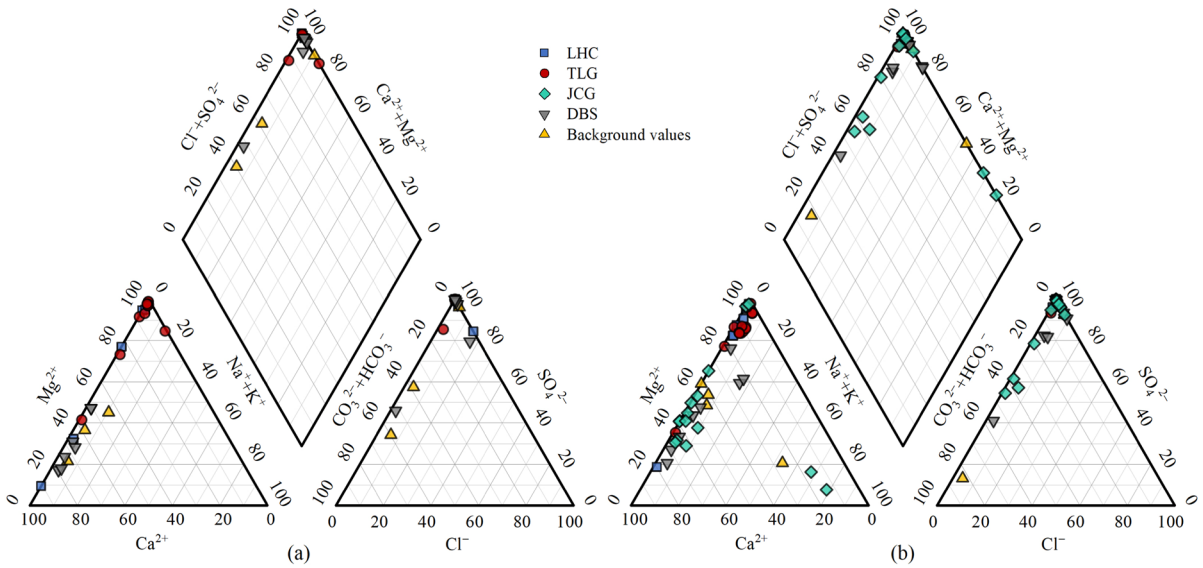


**Fig. 3** Piper diagrams of the cations and anions before (**a**) and after (**b**) the rain

Acid mine drainage index

The calculated results for the four mines were compared with uncontaminated springs in the study area and seriously contaminated mines in other countries (Table 2) (Sánchez España et al., 2005; Soltani et al., 2014). The calculated results indicate that the mean AMDI for the entire Baihe mine is 30.99 and for the other mines is 55.57. The mean AMDI for TLG and LHC is much lower than the mean AMDI for the uncontaminated springs and other mines. Therefore, Baihe mine must be classified as dangerous given the degree of AMD contamination.

Rainfall impact

Weather conditions, and especially precipitation, are the most significant external controlling factors in terms of the degree and range of AMD pollution. Comparing the pre- and post-rainfall results (Table 3), it was found that as the precipitation infiltrated to recharge the groundwater after the rain, indirectly affecting the water quantity entering the adit, the flow rates of water from the bottom floor and the top drip of the adit increase exponentially. As the flow rate increased, the AMD was diluted in most of the adits (e.g., DS7 and T4), resulting in lower concentrations of the main contaminants (e.g., Fe, $SO_4^{2-}$ and Mn). For a few adits (e.g., TL3 and TL1), the precipitation primarily affected the water–filled state of the surrounding rock, causing more joint fractures to start seeping, enlarging the water–sulfide mineral contact area to form more AMD. The increase in flux was not sufficient to dilute the amount of new AMD contamination generated by oxidation and leaching, resulting in higher contaminant concentrations after the rain (Mayo et al., 2000).

The influence of rainfall was studied by examining the concentration (or molar) ratios of dissolved constituents (Fig. 4). Oxidative dissolution of sulfide minerals (e.g., pyrite, chalcopyrite, and sphalerite) is the primary geochemical process in the mine adit; the concentration ratios of relevant contaminants and $SO_4^{2-}$ should not differ significantly before and after the rain under the dominant control of oxidative dissolution of sulfide minerals. The concentration ratio of Fe/$SO_4^{2-}$, Zn/ $SO_4^{2-}$, Mn/ $SO_4^{2-}$, and Cu/ $SO_4^{2-}$ did not change significantly before and after the rain overall, indicating that the concentration changes of Fe, Zn, Mn, and Cu before and after the rain were mainly caused by rainfall dilution and the enhancement of water–sulfide mineral interaction. However, the concentration ratio of Pb/ $SO_4^{2-}$ and Cd/ $SO_4^{2-}$ decreased overall after rain, and

**Table 2** Comparison of AMDI score of Baihe mine with uncontaminated springs and three mine sites

| Value | DBS | JCG | LHC | TLG | Baihe mine | Unpolluted spring | Animas district mine | Corta Atalaya mine | Darrehzar copper mine |
|---|---|---|---|---|---|---|---|---|---|
| Min | 1.78 | 0.20 | 1.78 | 0.79 | 0.20 | 87.11 | – | – | – |
| Max | 85.05 | 89.20 | 60.49 | 60.49 | 89.20 | 100.00 | – | – | – |
| Mean | 46.14 | 52.77 | 17.95 | 7.09 | 30.99 | 91.71 | 59.29 | 75.69 | 31.73 |

**Table 3** Comparison of concentration of pollution factors before and after rain in typical mine adits

| Adit | Stage | Flow rate | pH | Fe | $SO_4^{2-}$ | TDS | Mn | $NH_4^+$ | $COD_{Cr}$ | Se | As |
|---|---|---|---|---|---|---|---|---|---|---|---|
| | | ($m^3$/d) | | (mg/L) | (mg/L) | (mg/L) | (mg/L) | (mg/L) | (mg/L) | (mg/L) | (mg/L) |
| DS7 | Pre | 0.527 | 1.72 | 2.22E+03 | 9.29E+03 | 1.20E+04 | 2.80E+01 | 7.08E+01 | 2.38E+02 | 4.49E–01 | 5.12E–01 |
| | Post | 0.755 | 1.87 | 2.18E+03 | 5.92E+03 | 8.34E+03 | 3.06E+01 | 9.02E+01 | 1.64E+02 | 3.99E–01 | 4.96E–01 |
| T4 | Pre | 1.16 | 1.38 | 1.02E+04 | 3.35E+04 | 4.49E+04 | 8.63E+01 | 2.60E+00 | 1.81E+02 | 8.60E–02 | 3.60E–01 |
| | Post | 2.72 | 1.59 | 6.05E+03 | 1.92E+04 | 2.57E+04 | 5.74E+01 | 2.19E+02 | 1.87E+02 | 5.43E–01 | 2.22E+00 |
| TL3 | Pre | 6.577 | 1.9 | 5.43E+03 | 2.01E+04 | 2.65E+04 | 5.48E+01 | 1.00E+00 | 3.72E+02 | 2.00E–02 | 1.70E–01 |
| | Post | 20.74 | 1.8 | 6.39E+03 | 2.05E+04 | 2.73E+04 | 6.51E+01 | 1.67E+02 | 1.10E+02 | 6.10E–01 | 2.76E+00 |

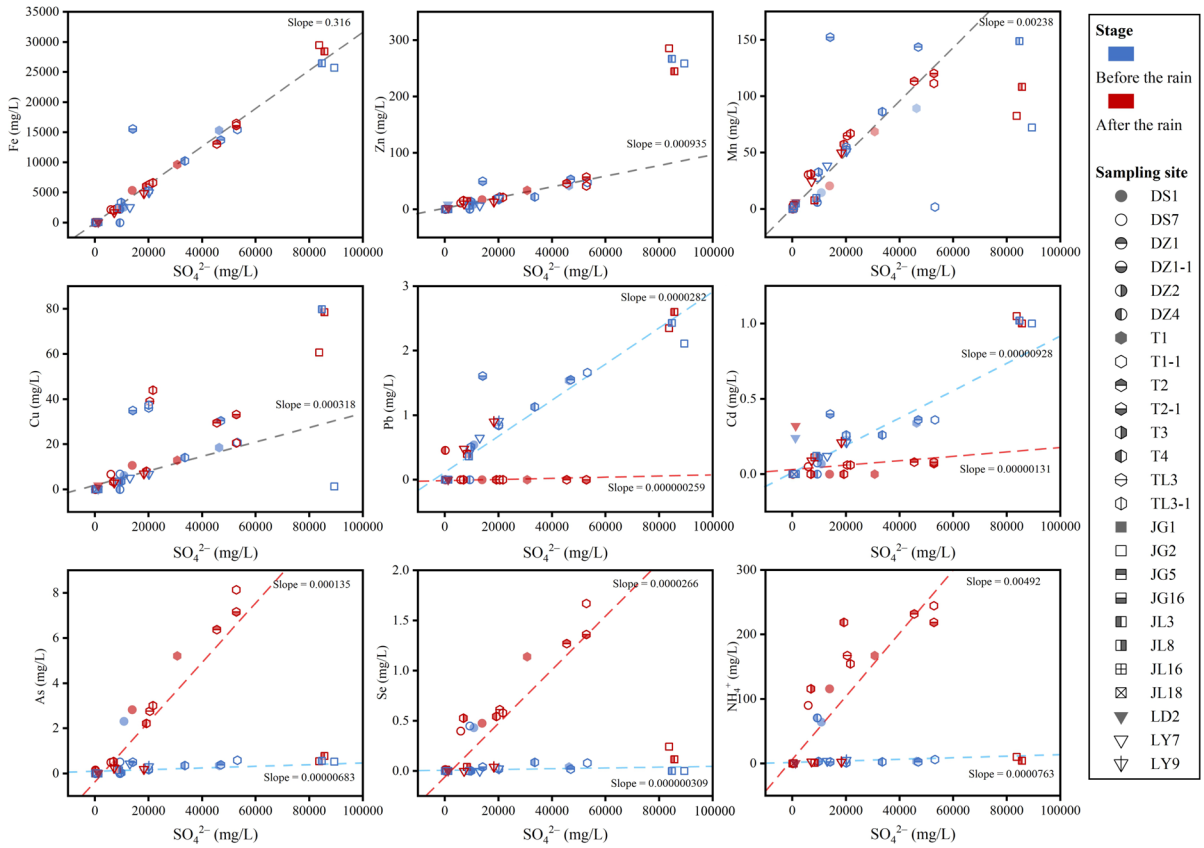


**Fig. 4** Concentration ratios between $SO_4^{2-}$ and several contaminants in the sampling sites before and after rain. The lines show the representative slope values (gray line: before and after the rain, blue line: before the rain, red line: after the rain)

the concentration ratio of As/ $SO_4^{2-}$, Se/ $SO_4^{2-}$ and $NH_4^+$/ $SO_4^{2-}$ increased overall after rain. This suggests that the solubility of these contaminants may be related to other geochemical behaviors rather than to the intensity of sulfide mineral oxidation. These changes in concentration ratios may be due to adsorption or co-precipitation of these contaminants by secondary minerals of Fe, such as As and Se, which are affected by stronger wash-out and dilution effects due to increased flux, resulting in their re-dissolution in water from Fe secondary minerals and an overall increase in their concentration (Davila et al., 2021; Sarmiento et al., 2009).

In the DBS and TLG, $NH_4^+$ concentrations increased abnormally after the rain, at the T4 adit entrance from 2.6 mg/L to 219 mg/L. To understand the causes of high $NH_4^+$ concentration, the $NO_3$/Cl-Cl method was used to identify sources of inorganic N (IN) pollution, which is mainly influenced by anthropogenic factors such as fertilizer inputs from agricultural activities, industrial and agricultural sewage discharges, and irrational irrigation (Kim et al., 2015). The high concentrations of $Cl^-$ and low $NO_3^-/Cl^-$ ratio of water samples could be attributed to manure and sewage; a low concentration of $Cl^-$ and high $NO_3^-/Cl^-$ ratio can be linked to chemical fertilizer; a low $Cl^-$ concentration and low $NO_3^-/Cl^-$ ratio can be linked to rock and soil organics (Feng et al., 2023; Torres-Martínez et al., 2021). In this study, water samples showed $Cl^-$ concentrations ranging from 1.57 to 55.8 mg/L, suggesting that manure and sewage are unlikely sources of IN contamination. Figure 5 shows that the source of IN contamination in AMD from DBS and TLG mine sites is rock and soil organics, while the sources of IN contamination in AMD from LHC and JCG mine sites are chemical fertilizer and rock and soil organics, which may be related to the presence of agricultural activities in the

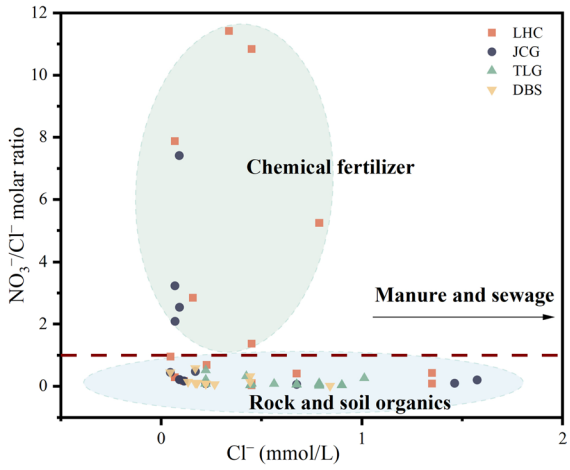


**Fig. 5** Scatter plots of the $NO_3^-/Cl^-$ ratio and $Cl^-$ molar concentration

upstream of LHC and JCG two mines. The IN from chemical fertilizers inputs into groundwater and infiltrates through cracks in mine adits. The phenomenon of increased $NH_4^+$ concentration is probably due to the large overlying aeration zone of the adit before the rain, which increased the release of $NH_4^+$ from microbial degradation and the enrichment of $NH_4^+$ by the negatively charged soil particles. After the rain, the precipitation dissolves the $NH_4^+$ adsorbed by the soil during infiltration (Liu et al., 2021), resulting in a large amount of $NH_4^+$ entering the adit with the groundwater. In addition, Fe(II) facilitates the conversion of nitrate nitrogen to ammonia nitrogen, leading to an abnormal increase in $NH_4^+$ concentration after the rain in the high Fe-concentration AMD environment.

## Correlation between contamination factors

Fe and $SO_4^{2-}$, as the main pollution factor, showed a strong positive correlation with each other ($r=0.97$), and the mean value of $Fe/SO_4^{2-}$ was 0.30 (Fig. 6a). When the $Fe/SO_4^{2-}$ ratio was approximately 0.29, it indicates that pyrite was oxidizing and higher than 0.29 indicates a tendency toward the dissolution of secondary minerals of Fe (54% of the total water samples), and lower than 0.29 indicates a tendency for Fe precipitation to occur (46% of the total water samples) (Cánovas et al., 2016). Dissolution/precipitation of Fe secondary mineral led to the release/storage of acidity, which was a key factor in controlling heavy metal concentrations in AMD (Liu et al., 2018). Furthermore, water typology at four mine sites was determined using Ficklin diagram (Fig. 6b); there was a trend of decaying heavy metal concentrations in AMD with increasing pH under the combined influence of both acid production and acid storage processes (Ficklin et al., 1992; Sarmiento et al., 2009). Most TLG and LHC water samples plot in the

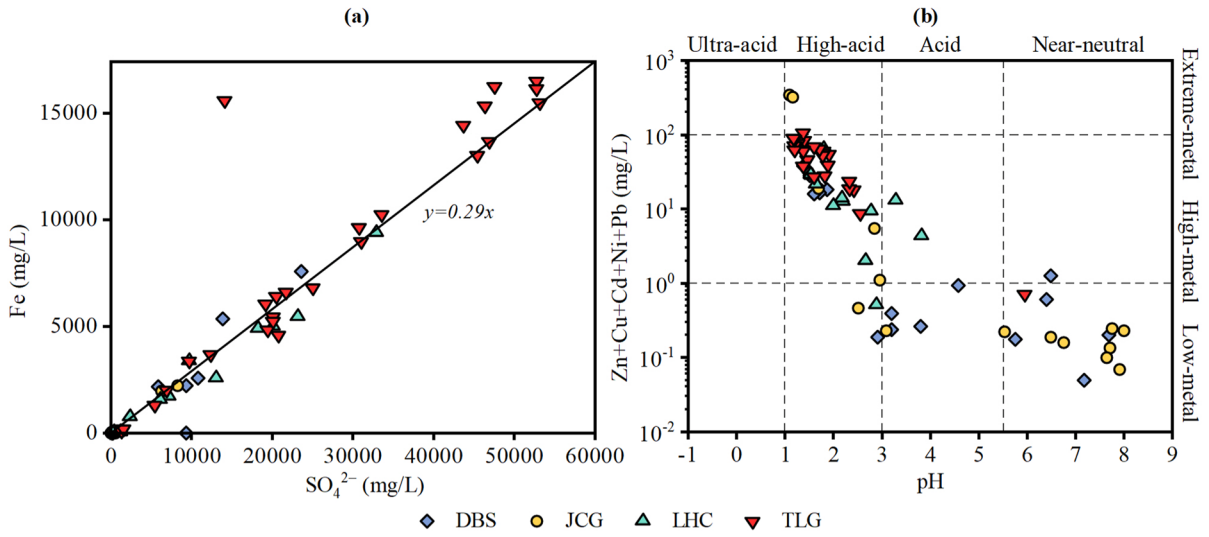


**Fig. 6** Relationship between **a** $SO_4^{2-}$ and Fe, and **b** Ficklin diagram

high-acid, high-metal region, while most DBS and JCG water samples plot in the acid and near-neutral, low-metal region.

Meanwhile, Fe, $SO_4^{2-}$ and Mn ($r=0.73$ with Fe, $r=0.70$ with $SO_4^{2-}$), Zn ($r=0.86$ with Fe, $r=0.83$ with $SO_4^{2-}$), Pb ($r=0.73$ with Fe, $r=0.70$ with $SO_4^{2-}$), Cu ($r=0.82$ with Fe, $r=0.79$ with $SO_4^{2-}$), and Cd ($r=0.74$ with Fe, $r=0.72$ with $SO_4^{2-}$) also show significant positive correlations (Fig. 7). This indicates that the release behavior of these heavy metal elements is mainly controlled by the pyrite oxidation. Furthermore, the associated minerals, such as chalcopyrite and arsenopyrite, dissolved and released heavy metal elements in contact with AMD (Shum & Lavkulich, 1999). These heavy metal ions were less affected by adsorption in acidic water; the release amount was much smaller than the adsorption amount, resulting in the formation of a large amount of Fe ions and $SO_4^{2-}$, and the concentration of heavy metal ions was also abnormally high.

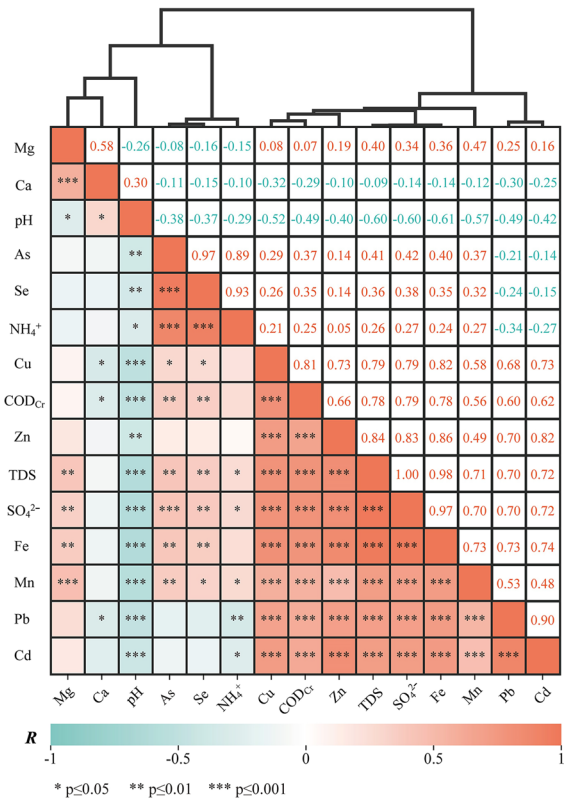


**Fig. 7** Heat map and clustering results of the correlation between AMD major contamination factors

pH shows a significant negative correlation with most of the contaminants, the pH value decreases while the concentration of contaminants increases, which is mainly attributed to the release of a large amount of $H^+$ during the oxidation of pyrite (Bigham et al., 1996a). The correlation coefficients of $NH_4^+$/As, $NH_4^+$/Se, and As/Se were 0.89, 0.93, and 0.97, respectively. This relevance is mainly attributed to the fact that $NH_4^+$, As, and Se are all influenced by rainfall, and the concentrations of the three pollutants increase after the rain, while the concentrations are smaller before the rain.

The clustering analysis characterized and classified each contamination factor of AMD and showed the hydrogeochemical correlation among the factors (Grande et al., 2010). The pollution factors were grouped according to the Euclidean distance, majorly into three clusters: (1) cluster comprising Mg, Ca, and pH related to the carbonate dissolution; (2) cluster comprising As, Se, and $NH_4^+$ related to the influence of rainfall, and (3) cluster comprising Cu, Zn, Fe, Mn, $SO_4^{2-}$, TDS, $COD_{Cr}$, Pb, and Cd enriched from the sulfate minerals dissolution. The cluster analysis also demonstrates the strong relationship between Fe, $SO_4^{2-}$, and TDS. This is evident in the high proximity observed in the cluster results. Somewhat more discrete are the proximity relationships between Pb and Cd. The Euclidean distances between As and Se were also small because of the similarity of the metalloid release behavior in AMD. The clustering results were well verified the correlation among the above pollution factors.

## Mineralogy of AMD sediments

Sediment sampling was carried out at 3 m, 23 m, 43 m, 58 m, 74 m, and 84 m from the entrance of the chamber in the typical mining adit J16. Most of the sediments were ochre yellow and yellowish brown, which are typical characteristics of Fe-rich and S-rich.

After the PDF card comparison, the presence of Fe hydroxyl sulfate minerals and Fe hydroxyl oxides was detected at each site, such as jarosite, schwertmannite, and goethite (Fig. 8). These secondary minerals have large specific surface areas, which can adsorb, deposit, and co-precipitate heavy metals under different pH to achieve self-purification of AMD (Baleeiro et al., 2018; Burton et al., 2007). XRD results showed that goethite was detected at all

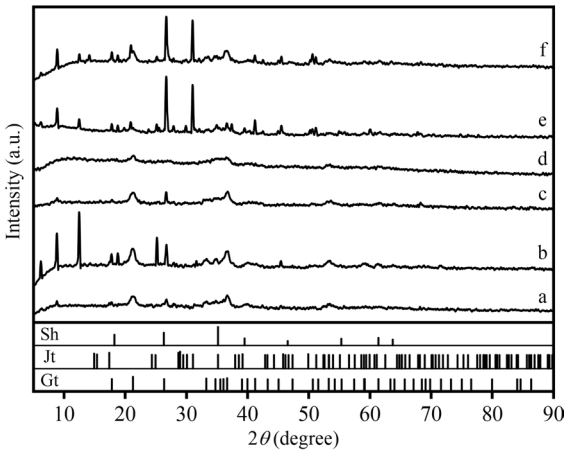


**Fig. 8** X-ray powder diffraction pattern of sediments at different distances from adit entrance in adit J16 (line a: 3 m; line b: 23 m; line c: 43 m; line d: 58 m; line e: 74 m; line f: 84 m. Gt: goethite, Jt: jarosite, Sh: schwertmannite)

**Table 4** Mineralogy of sediments and pH of AMD in the adit J16

| # | Distance (m) | Ferrous secondary mineral | pH |
|---|---|---|---|
| a | 3 | Ht, Jt, Gt | 2.28 |
| b | 23 | Ht, Gt | – |
| c | 43 | Ht, Jt, Gt, Sh | – |
| d | 58 | Ht, Gt | 2.59 |
| e | 74 | Gt | 7.4 |
| f | 84 | Gt | – |

Ht—hematite, Gt—goethite, Jt—jarosite, Sh—schwertmannite, – no detectable water

sites, as well as silicate and aluminosilicate minerals such as biotite and kaolinite. Gypsum was also found in the sediments due to the high $SO_4^{2-}$ and $Ca^{2+}$ concentrations in the AMD. The main secondary minerals of Fe detected at each site are found in Table 4. Fe sulfides such as pyrite and marcasite were detected at 3 m, with the most obvious peak of goethite. The chlorite and ferroan clinochlore, with obvious kaolinite diffraction peaks, were also detected at 23 m, but without detecting Fe sulfides. The XRD pattern of 43 m showed the most species of Fe secondary minerals and Fe sulfides. Dolomite and chlorite were also detected at 74 m and 84 m, and since AMD did not form at these sites, only goethite and Fe sulfides were detected. From the end to the entrance of the adit, the species of secondary minerals of Fe gradually increased as AMD formed and then decreased as the metastable minerals transitioned to stable minerals.

## Geochemical modeling

Inverse modeling is the process of extrapolating the water–rock interactions in a system, based on known information about the water quality of the initial and final water samples. Also, the complex reactions that occur among different minerals are quantified by inverse modeling. In the case of J16, the initial water sample from the top drip at 77.4 m, a site with similar water quality to the background values in the study area, was directly recharged by the upstream fissure water and then infiltrating into the sediment layer at the bottom floor of the adit. The final water sample was taken from the bottom flow at the entrance of the adit, indicating seepage through the sediment layer. The initial and final water samples are limited by the mineral phases in the sedimentary layers. The potential mineral phases were constrained according to the dissolution/precipitation trend of the SI data (logarithm of the quotient of ion activity product (IAP) and solubility product ($K_{SP}$)). Saturation indices of main mineral phases related to hydrogeochemical processes in mine adits are found in Fig. 9; for SI = 0, there is equilibrium between the solid mineral and the aqueous phase; negative and positive SI values reflect undersaturation and supersaturation, respectively. The dissolution/precipitation state of minerals changes at different distances in the mine adit as the hydrogeochemical processes evolve. The model optimal solution was selected by the sum of residuals and maximum fractional error of the inversion results calculated by PHREEQC. To determine the changes in Fe and S elements of the pathway, pyrite, hematite, jarosite, schwertmannite, goethite, and ferrihydrite were selected as the main mineral phases based on XRD analysis of the sediment and SI data. Considering the effect of carbonate dissolution, calcite, dolomite, and gypsum were selected. Epsomite was selected as the main mineral affecting the increase in Mg concentration. Three optimal inverse models for the phase mole transfer of the selected simulated minerals along the AMD formation pathway are found in Table 5. The inverse modeling results showed that oxidative dissolution of sulfide minerals, interconversion of Fe-hydroxy secondary minerals, precipitation

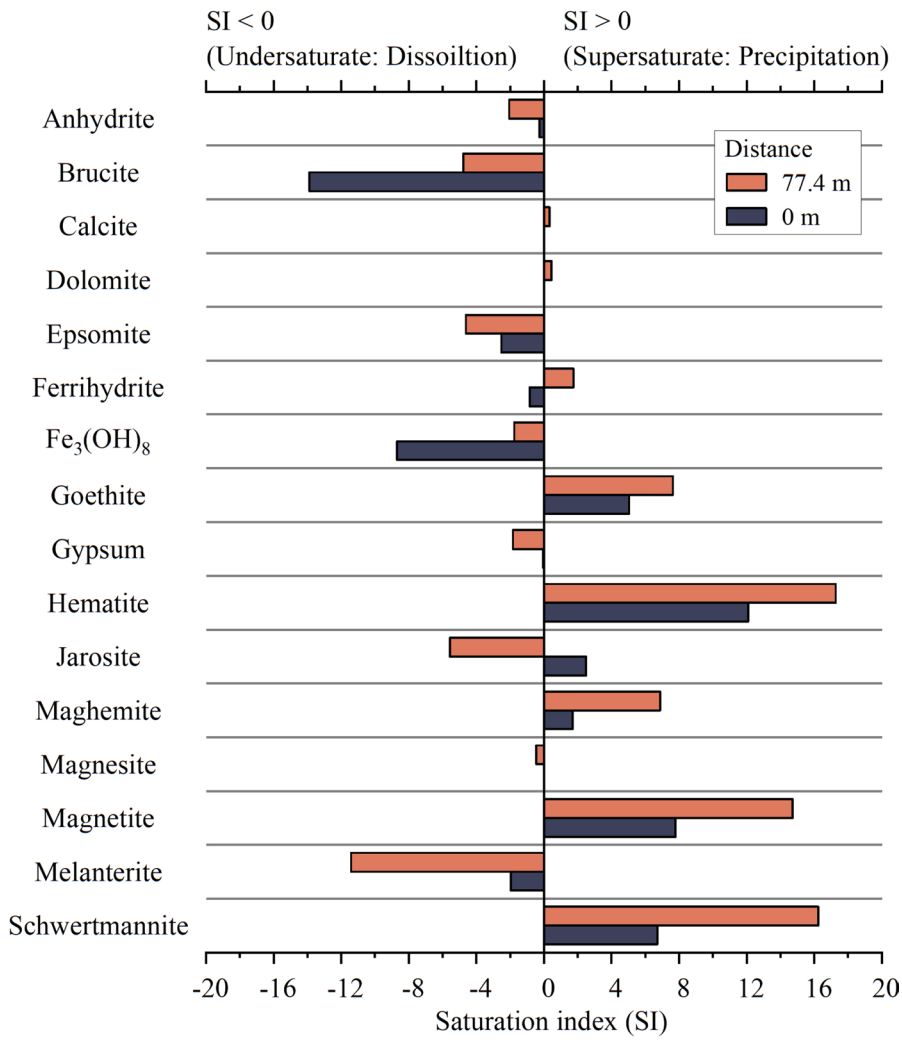


**Fig. 9** Saturation indices of bottom flow at different distances from adit entrance in adit J16

of gypsum, and neutralization by calcite were the main geochemical reactions in the mine adit. Some inverse modeling studies investigating natural attenuation pathways for AMD have observed the presence of hydrogeochemical processes, such as precipitation of Fe secondary minerals (ferrihydrite, goethite, and schwertmannite) and dissolution of calcite (Asta et al., 2015; Sharif et al., 2008). The similarities of calcite dissolution confirm that calcite may function as a major neutralizer in the AMD pathway. Outside the mine adit, the overall AMD contamination is decreasing, and Fe secondary minerals continue to precipitate during the natural attenuation. This study simulates the formation of AMD in the mine adit, where Fe secondary minerals undergo a variety of reactions such as dissolution, precipitation, and transformation due to the instability in hydrogeochemical conditions. As the pH in the mine adit is significantly lower, the modeling results show the precipitation of jarosite and the absence of ferrihydrite.

It is important to mention that schwertmannite in the simulation results was dissolved (positive mole transfer number) because the acidic environment influenced by pH and Eh in the J16 was not suitable for schwertmannite formation. XRD results detected schwertmannite only at site 43 m, where AMD was continuously injected and slow moved, which was suitable for schwertmannite deposition. Schwertmannite is a metastable mineral (Acero et al., 2006); when the pH, Eh, temperature, and other conditions of AMD change, they will cause the transformation of schwertmannite to the more stable jarosite and

**Table 5** Inverse modeling along the flow path J16 77.4–0 m

| Mineral phases | Phase mole transfers J16 77.4–0 m | | |
|---|---|---|---|
| Calcite | 2.68E + 01 | − 2.33E − 02 | 2.16E − 02 |
| Dolomite | − 1.34E + 01 | 9.82E − 03 | − 1.26E − 02 |
| Goethite | − 2.63E + 01 | − 2.55E − 01 | − 2.55E − 01 |
| Epsomite | 1.34E + 01 | – | 2.24E − 02 |
| Gypsum | − 1.34E + 01 | 2.24E − 02 | – |
| Ferrihydrite | – | – | – |
| Jarosite | – | − 1.89E − 05 | − 1.89E − 05 |
| Schwertmannite | 3.81E − 02 | 3.62E − 02 | 3.62E − 02 |
| Hematite | 1.30E + 01 | – | – |
| Pyrite | 1.90E − 03 | 1.90E − 03 | 1.90E − 03 |

3 possible models were obtained for J16 77.4–0 m. Thermodynamic database used: WATEQ4F.dat values are in mol/kg $H_2O$. Positive (mass entering water) and negative (mass leaving water) phase mole transfers indicate dissolution and precipitation, respectively. – no mass transfer

goethite (Eqs. (3) and (4)). The transformation is equivalent to the re-dissolution of schwertmannite into the liquid phase in the whole path calculation.

$$Fe_8O_8(OH)_6SO_4 + 2H_2O \Leftrightarrow 8FeOOH + SO_4^{2-} + 2H^+ \quad (3)$$

$$3Fe_8O_8(OH)_6SO_4 + 6H_2O + 8K^+ + 18H^+ + 13SO_4^{2-} \Leftrightarrow 8KFe_3(SO_4)_2(OH)_6 \quad (4)$$

The presence of chlorite detected at several sites indicates that chlorite may also be involved in the neutralization of AMD in the adit, in addition to calcite and dolomite (Wu et al., 2006). Chlorite, which has been formed under metamorphic conditions, is less stable than most of the other clays under acidic weathering conditions and therefore may be rapidly altered (Brandt et al., 2003). Primary chlorites can transform into regularly and irregularly interstratified vermiculite/smectite because of preferential leaching of certain cations from the chlorite structure. Vermiculite was detected in the XRD results of the sediments, and its presence can prove that chlorite is involved in the neutralization of AMD because it is a phase transformed by chlorite in acidic environments. The inverse modeling results showed a difference in dissolution/precipitation trends between calcite and dolomite in AMD formation, which was consistent with the detection of dolomite but not calcite in the XRD results. The absence of epsomite dissolution mainly caused the difference in the second optimal model. The absence of an external source of Mg within the system resulted in an increased Mg concentration that could only be supplemented by the dissolution of dolomite, which led to the precipitation of calcite. However, there were multiple Mg-bearing dissolvable minerals in the adit, so the first and third carbonate dissolution/precipitation trends were more reasonable. Thus, calcite and chlorite may be the major neutralizing minerals for AMD within the mine adit, rather than calcite and dolomite as commonly believed.

## Special sources of AMD

Most of the studied adits provided perfect oxidation zones since the adits were left open for their entire length due to the lack of post-abandonment remediation in the study area. The air oxygen concentration was 20.9%, and water dissolved oxygen concentrations ranged from 2.21 to 8.53 mg/L. On the other hand, the exposure of the adit has resulted in significant weathering of the rock. The joint fractures in the fracture zone are further developed and constitute the main leakage channels for the adit, allowing groundwater to infiltrate through the joint fractures into the adit and contact with the pyrite ore bodies. The above conditions provide the environment for pyrite oxidation.

Depending on the main oxidant, the pyrite oxidation reaction is divided into two stages (initial acid production stage and cyclic acid production stage). At the initial acid production stage (Eq. (5)), the oxidation rate of pyrite is slow, but the pH of the water gradually decreases as the reaction continues (Nordstrom & Alpers, 1999). When pH < 5, the reaction product Fe(II) comes into sufficient contact with oxygen, accompanied by the powerful catalytic effect of microorganisms (Fan et al., 2022); Fe(II) will be oxidized to Fe(III) (Eq. (6)). Then, the acid production changes into a cyclic acid production stage, with Fe(III) gradually replacing oxygen as the main oxidant (Eq. (7)).

$$FeS_2 + 3.5O_2 + H_2O \rightarrow Fe^{2+} + 2SO_4^{2-} + 2H^+ \quad (5)$$

$$Fe^{2+} + 0.25O_2 + H^+ \rightarrow Fe^{3+} + 0.5H_2O \quad (6)$$

$$FeS_2 + 14Fe^{3+} + 8H_2O \rightarrow 15Fe^{2+} + 2SO_4^{2-} + 16H^+ \quad (7)$$

Fe(III) is a powerful oxidant and can oxidize pyrite in an anaerobic environment (Grande et al., 2016). The oxidation rate increases exponentially compared to the initial acid production stage, likely due to the microbial catalysis (mainly *Acidithiobacilus thiooxidans* and *Acidithiobacilus ferroxidans*), resulting in a rapid decrease in pH (Dong et al., 2023; Galhardi & Bonotto, 2016). Once entering the cyclic stage, with sufficient oxygen and water in the environment, the Fe(II) formed by the reaction can continue to be oxidized again to form Fe(III), further oxidizing the pyrite. In addition, the presence of carbonate minerals, such as calcite and dolomite, can neutralize AMD and remove heavy metals (Holmström et al., 2001).

In addition, the lack of carbonate rocks is also essential for the occurrence of AMD. In the study area, the carbonate rocks are either poorly formed or consumed, and most water samples have $HCO_3^-$ concentrations ≈ 0 mg/L. The neutralizing effect of the carbonate rocks on AMD was limited. The acid production was greater than the neutralizing effect, which was sufficient for AMD formation and heavy metal release within the adits.

AMD was not generated solely through the oxidation of pyrite in some of the mines. The pore aquifer was formed by the artificial deposition of waste rock in linear or laminated patterns at the mine site, which showed low groundwater reservoir volume, but high permeability. Precipitation and surface water can easily infiltrate to recharge the aquifer. Moreover, this aquifer was formed by the accumulation of pyrite slag, which was a source of contamination. Consequently, the water contacts the slag during infiltration and oxidation occurs to form AMD, which then enters the adit through the joint fracture channels (Fig. 10).

To verify the above assumptions, samples were taken from both the bottom flow (a confluence of multiple water sources) and the top drip (the most closely associated with the overlying groundwater recharge). For example, the main chamber of DZ1 was 82 m deep and had two branches, with 0–60 m of the main chamber and the entire second branch being located under the waste rock dump. The measurements for Eh and pH were taken at 5-m intervals throughout the adit. The Eh and pH were similar to the background values for the 60–80 m of the main chamber. The AMD generated in the overlying aquifer infiltrates due to the overlying waste rock dump starting from 60 m in the main chamber, causing the top

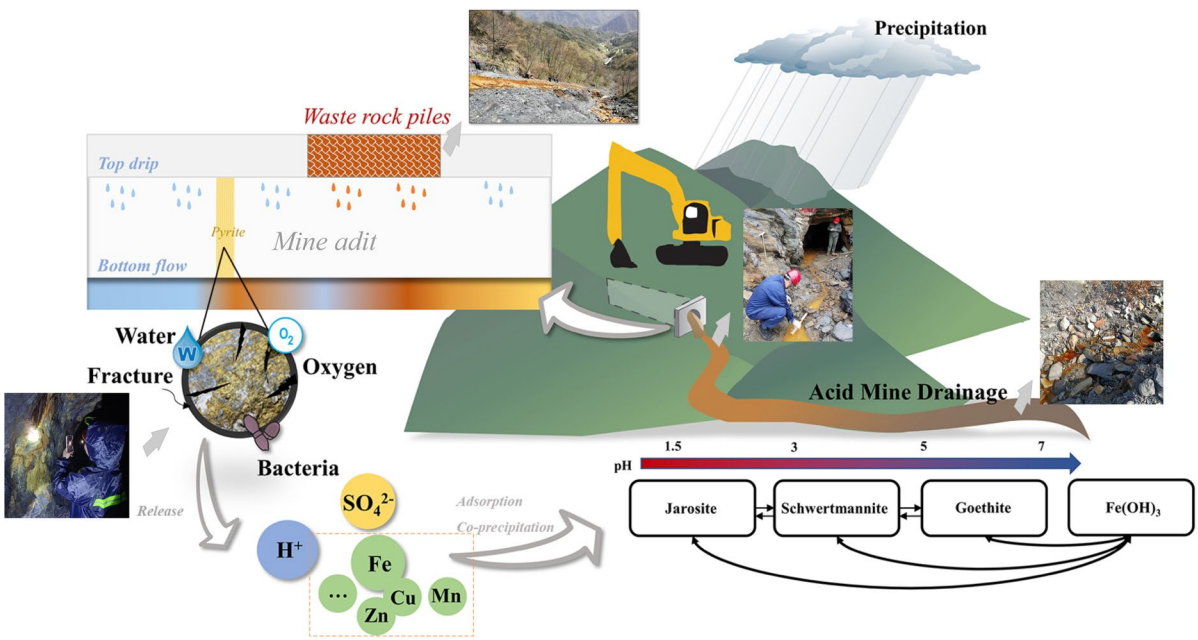


**Fig. 10** Generation of AMD and geochemical processes occurring in the mine adit

drip to change in pH and Eh and continuing to affect the bottom flow in the subsequent 0–60 m. The ore bodies in DZ1 were mainly located in the fault zone at 69.5 m from the main chamber, but the bottom flow and top drip did not change significantly from 65 to 70 m without the occurrence of AMD. This may be caused by the small thickness of the ore body, which did not contact with water, or the influence of alteration of the ore body.

Eh and pH were also measured for comparison within TL1, an adit with no overlying waste rock dump with a main chamber 130 m deep where the mining pit is located at 130 m. The results showed that both the bottom flow and the top drip were strongly acidic and oxidizing due to the presence of pyrite ore bodies in the pit at 130 m. The bottom flow rate was 1.05–1.12 $m^3$/d from 98 to 130 m, with only a few drips from the top and sidewalls, which was close to neutral water and had minimal impact on the hydrochemical characteristics of the bottom flow AMD. The stalactites were well developed from 88–98 m, and at 92.7 m there was a beaded drip along the stalactites with an $HCO_3^-$ concentration of 240.7 mg/L, pH = 6.22 and flow rate varied between 0.72 and 0.97 $m^3$/d close to the bottom flow. The subsequent 0–88 m had no overlying AMD infiltration; thus, the top drip was neutral or even alkaline, which diluted and neutralized the bottom flow. However, the pH and Eh of the bottom flow significantly changed at 50 m of TL1 under the influence of the pyrite deposit. The first branch of DZ1, which also does not have an overlying waste rock dump, has an $HCO_3^-$ concentration of 240.7 mg/L and high $Ca^{2+}$ and $Mg^{2+}$ concentrations, indicating that the presence of dissolved carbonates, but the flow rate is only 2.31–2.60 $m^3$/d, which is much lower than the flow rate in the main chamber thus providing little dilution and neutralization.

The comparison revealed that the pH bottom flow > top drip for the entire distance of DZ1 and the opposite for TL1. Eh in both chambers generally showed bottom flow > top drip, except at the confluence of DZ1 (Fig. 11). The pH and Eh curves of the bottom flow and top drip in DZ1 were similar, suggesting that the dominant factor in the generation of AMD was the infiltration of AMD from the overlying layer, whereas the pH and Eh curves of the bottom flow and top drips in TL1 were different, with the main regulating variable being the oxidation of pyrite bodies. The hydrochemical characteristics of the AMD generated in the overlying layer differed from the AMD generated in the adit due to the acidity consumed during the infiltration process and the strong sorption of heavy metal ions by the soil particles (Alumaa et al., 2002; Bradl, 2004), which was characterized by higher pH and lower concentrations of contaminants.

## Conclusions

The AMD, in abandoned adits of Baihe mine, can be characterized by low pH and high TDS, with extremely high concentrations of Fe and $SO_4^{2-}$. The

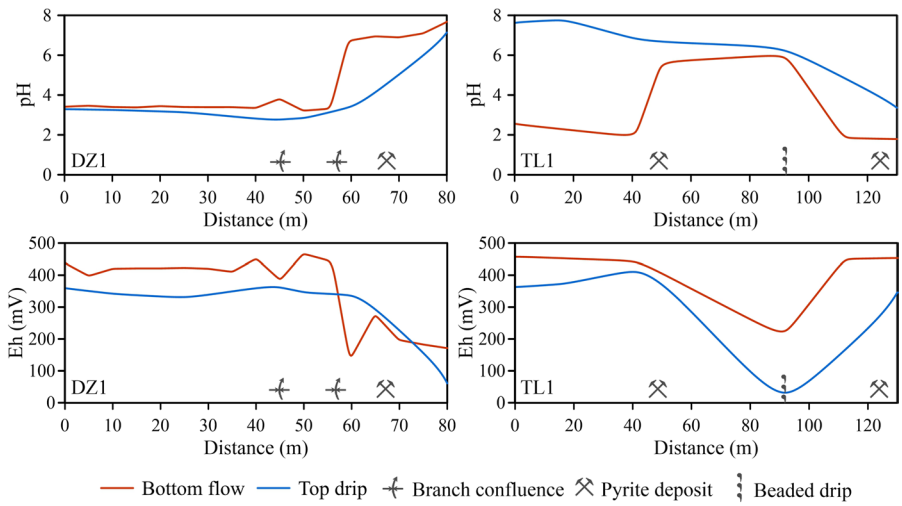


**Fig. 11** Variation in pH and Eh values with distance from adit entrance in the mine adit DZ1 and TL1

hydrochemical type of AMD was $SO_4$–Ca–Mg, $SO_4$–Ca, and $SO_4$–Mg, while precipitation reduced concentrations of the main contaminants in mine adits. The mean AMDI for the entire Baihe mine is 30.99, lower than the AMDI for the other seriously contaminated mines. Therefore, Baihe mine must be classified as dangerous given the degree of AMD contamination. The main pollution factors (i.e., Fe and $SO_4^{2-}$) showed a strong and positive correlation with each other. The release behavior of heavy metals was controlled by the oxidation of sulfide minerals (mainly pyrite), while its concentration showed a significant positive correlation with Fe and $SO_4^{2-}$. Moreover, the contaminant concentrations changed after the rain affected by flow rates of adit water, dissolution/precipitation of secondary minerals and the overlying zone of aeration, and $NH_4^+$ concentrations increased abnormally after the rain, which can be attributed to the stability and enrichment of $NH_4^+$ in high Fe concentration environments. Since multiple Fe-hydroxy secondary minerals (mainly goethite) are present in the AMD formation path, the species of Fe-hydroxy secondary minerals initially increased and later decreased due to the transformation of metastable minerals to stable minerals.

The mineral phase transformations from the inverse modeling match the XRD results, and the main hydrogeochemical processes within the adit can be inferred by XRD results combined with inverse modeling. The inverse modeling results showed that oxidative dissolution of sulfide minerals, interconversion of Fe-hydroxy secondary minerals, precipitation of gypsum, and neutralization by calcite were the main geochemical reactions in the mine adit. In the AMD environment, calcite dissolved while dolomite precipitated, and chlorite might be the dominant neutralizer of AMD in the adit with calcite.

Most of the adits in the study area were not obstructed, which led to adequate aeration in the adit and the significant development of the fractured zone. This allowed fissure water to enter the adit and react with the pyrite (ore bodies and waste), creating native AMD in the adit. Furthermore, the overlying waste rock dumps were exposed to the environment, allowing precipitation to pass through the dumps to form acidic water and infiltrate into the adit, which was also a significant source of AMD. Treating such adits should prioritize addressing external pollution sources rather than the mine adit itself.

**Acknowledgements** This research was mainly supported by the Geological and Mineral Engineering Survey Institute, Shaanxi. All the authors sincerely thank the researchers and workers for their help. We also thank the anonymous referees for their thorough reviews and constructive comments. They have helped improve the quality of the original manuscript.

**Author contributions** WC took part in investigation; formal analysis; methodology; writing—original draft; writing—review and editing. XK involved in investigation; methodology; writing—review and editing. WW took part in resources; writing—reviewing and editing. PL took part in investigation; formal analysis. All authors contributed to the article and approved the submitted version.

**Funding** The authors did not receive support from any organization for the submitted work.

**Data availability** The data used during the current research are available from the corresponding author on reasonable request.

**Declarations**

**Conflict of interest** The authors declare no competing interests.

**Ethics approval** This article does not involve studies with animals or human participation.

## References

Acero, P., Ayora, C., Torrentó, C., & Nieto, J.-M. (2006). The behavior of trace elements during schwertmannite precipitation and subsequent transformation into goethite and jarosite. *Geochimica Et Cosmochimica Acta, 70*, 4130–4139. https://doi.org/10.1016/j.gca.2006.06.1367

Acharya, B. S., & Kharel, G. (2020). Acid mine drainage from coal mining in the United States: An overview. *Journal of Hydrology, 588*, 125061. https://doi.org/10.1016/j.jhydrol.2020.125061

Akcil, A., & Koldas, S. (2006). Acid mine drainage (AMD): Causes, treatment and case studies. *Journal of Cleaner Production, 14*, 1139–1145. https://doi.org/10.1016/j.jclepro.2004.09.006

Alumaa, P., Kirso, U., Petersell, V., & Steinnes, E. (2002). Sorption of toxic heavy metals to soil1 1Following a presentation given as part of the International Congress on Environmental Health and the 4th Annual Meeting of the International Society of Environmental Medicine (ISEM), 1–4 October, 2000, Hannover Germany. *International Journal of Hygiene and Environmental Health, 204*, 375–376. https://doi.org/10.1078/1438-4639-00114

Asta, M. P., Calleja, M. L., Pérez-López, R., & Auqué, L. F. (2015). Major hydrogeochemical processes in an acid mine drainage affected estuary. *Marine Pollution Bulletin, 91*, 295–305. https://doi.org/10.1016/j.marpolbul.2014.11.023

Baleeiro, A., Fiol, S., Otero-Fariña, A., & Antelo, J. (2018). Surface chemistry of iron oxides formed by neutralization of acidic mine waters: Removal of trace metals. *Applied Geochemistry, 89*, 129–137. https://doi.org/10.1016/j.apgeochem.2017.12.003

Ball J. W., Nordstrom D. K. (1991). User's manual for WATEQ4F, with revised thermodynamic data base and text cases for calculating speciation of major, trace, and redox elements in natural waters. 91–183, Survey USG. http://pubs.er.usgs.gov/publication/ofr91183

Bigham, J. M., Schwertmann, U., & Pfab, G. (1996a). Influence of pH on mineral speciation in a bioreactor simulating acid mine drainage. *Applied Geochemistry, 11*, 845–849. https://doi.org/10.1016/S0883-2927(96)00052-2

Bigham, J. M., Schwertmann, U., Traina, S. J., Winland, R. L., & Wolf, M. (1996b). Schwertmannite and the chemical modeling of iron in acid sulfate waters. *Geochimica Et Cosmochimica Acta, 60*, 2111–2121. https://doi.org/10.1016/0016-7037(96)00091-9

Bradl, H. B. (2004). Adsorption of heavy metal ions on soils and soils constituents. *Journal of Colloid and Interface Science, 277*, 1–18. https://doi.org/10.1016/j.jcis.2004.04.005

Brandt, F., Bosbach, D., Krawczyk-Bärsch, E., Arnold, T., & Bernhard, G. (2003). Chlorite dissolution in the acid ph-range: A combined microscopic and macroscopic approach. *Geochimica Et Cosmochimica Acta, 67*, 1451–1461. https://doi.org/10.1016/S0016-7037(02)01293-0

Burton, E. D., Bush, R. T., Sullivan, L. A., & Mitchell, D. R. G. (2007). Reductive transformation of iron and sulfur in schwertmannite-rich accumulations associated with acidified coastal lowlands. *Geochimica Et Cosmochimica Acta, 71*, 4456–4473. https://doi.org/10.1016/j.gca.2007.07.007

Cánovas, C. R., Macías, F., & Pérez-López, R. (2016). Metal and acidity fluxes controlled by precipitation/dissolution cycles of sulfate salts in an anthropogenic mine aquifer. *Journal of Contaminant Hydrology, 188*, 29–43. https://doi.org/10.1016/j.jconhyd.2016.02.005

Caraballo, M. A., Macías, F., Rötting, T. S., Nieto, J. M., & Ayora, C. (2011). Long term remediation of highly polluted acid mine drainage: A sustainable approach to restore the environmental quality of the Odiel river basin. *Environmental Pollution, 159*, 3613–3619. https://doi.org/10.1016/j.envpol.2011.08.003

Chen, M., Lu, G., Wu, J., Sun, J., Yang, C., Xie, Y., Wang, K., Deng, F., Yi, X., & Dang, Z. (2020). Acidity and metallic elements release from AMD-affected river sediments: Effect of AMD standstill and dilution. *Environmental Research, 186*, 109490. https://doi.org/10.1016/j.envres.2020.109490

Chidambaram, S., Prasanna, M. V., Singaraja, C., Thilagavathi, R., Pethaperumal, S., & Tirumalesh, K. (2012). Study on the saturation index of the carbonates in the groundwater using WATEQ4F, in layered coastal aquifers of Pondicherry. *Journal of the Geological Society of India, 80*, 813–824. https://doi.org/10.1007/s12594-012-0210-0

Davila, J. M., Sarmiento, A. M., Aroba, J., Fortes, J. C., Grande, J. A., Santisteban, M., Cordoba, F., Leiva, M., & Luís, A. T. (2021). Application of a fuzzy logic based methodology to validate the hydrochemical characterization and determining seasonal influence of a watershed affected by acid mine drainage. *International Journal of Environmental Research and Public Health, 18*, 4693. https://doi.org/10.3390/ijerph18094693

Dong, Y., Lu, H., & Lin, H. (2023). Release characteristics of heavy metals in high-sulfur coal gangue: Influencing factors and kinetic behavior. *Environmental Research, 217*, 114871. https://doi.org/10.1016/j.envres.2022.114871

Fan, R., Qian, G., Li, Y., Short, M. D., Schumann, R. C., Chen, M., Smart, R. S. C., & Gerson, A. R. (2022). Evolution of pyrite oxidation from a 10-year kinetic leach study: Implications for secondary mineralisation in acid mine drainage control. *Chemical Geology, 588*, 120653. https://doi.org/10.1016/j.chemgeo.2021.120653

Feng, B., Zhong, Y., He, J., Sha, X., Fang, L., Xu, Z., & Qi, Y. (2023). Nitrogen sources and conversion processes in shallow groundwater around a plain lake (Northwest China): Evidenced by multiple isotopes and water chemistry. *Chemosphere, 337*, 139322. https://doi.org/10.1016/j.chemosphere.2023.139322

Ficklin W., Plumlee G., Smith K. & McHugh J. (1992). Geochemical classification of mine drainages and natural drainages in mineralized areas, *International symposium on water-rock interaction* (pp. 381–384).

Galhardi, J. A., & Bonotto, D. M. (2016). Hydrogeochemical features of surface water and groundwater contaminated with acid mine drainage (AMD) in coal mining areas: A case study in southern Brazil. *Environmental Science and Pollution Research, 23*, 18911–18927. https://doi.org/10.1007/s11356-016-7077-3

Grande, J. A., de la Torre, M. L., Cerón, J. C., Beltrán, R., & Gómez, T. (2010). Overall hydrochemical characterization of the Iberian Pyrite Belt. Main acid mine drainage-generating sources (Huelva, SW Spain). *Journal of Hydrology, 390*, 123–130. https://doi.org/10.1016/j.jhydrol.2010.06.001

Grande, J. A., De La Torre, M. L., Santisteban, M., Valente, T., Fernandez, J. P., & Pérez-Ostalé, E. (2016). Spatial evolution of an AMD stream in the Iberian Pyrite Belt: Process characterization and control factors on the hydrochemistry. *Hydrological Sciences Journal, 61*, 1503–1511. https://doi.org/10.1080/02626667.2014.983515

Gray, N. F. (1996). The Use of an Objective Index for the Assessment of the Contamination of Surface Water and Groundwater by Acid Mine Drainage. *Water Environment Journal, 10*, 332–340. https://doi.org/10.1111/j.1747-6593.1996.tb00061.x

Han, Y.-S., Youm, S.-J., Oh, C., Cho, Y.-C., & Ahn, J. S. (2017). Geochemical and eco-toxicological characteristics of stream water and its sediments affected by acid mine drainage. *CATENA, 148*, 52–59. https://doi.org/10.1016/j.catena.2015.11.015

Hermassi, M., Granados, M., Valderrama, C., Ayora, C., & Cortina, J. L. (2022). Recovery of rare earth elements from acidic mine waters: An unknown secondary resource. *Science of the Total Environment, 810*, 152258. https://doi.org/10.1016/j.scitotenv.2021.152258

Holmström, H., Salmon, U. J., Carlsson, E., Petrov, P., & Öhlander, B. (2001). Geochemical investigations of sulfide-bearing tailings at Kristineberg, northern Sweden, a few years after remediation. *Science of the Total*

*Environment, 273*, 111–133. https://doi.org/10.1016/S0048-9697(00)00850-0

Hu, J., Zhu, C., Long, Y., Yang, Q., Zhou, S., Wu, P., Jiang, J., Zhou, W., & Hu, X. (2021). Interaction analysis of hydrochemical factors and dissolved heavy metals in the karst Caohai Wetland based on PHREEQC, cooccurrence network and redundancy analyses. *Science of the Total Environment, 770*, 145361. https://doi.org/10.1016/j.scitotenv.2021.145361

Kim, D.-M., Kwon, H.-L., & Im, D.-G. (2023). Determination of contamination sources and geochemical behaviors of metals in soil of a mine area using Cu, Pb, Zn, and S isotopes and positive matrix factorization. *Journal of Hazardous Materials, 447*, 130827. https://doi.org/10.1016/j.jhazmat.2023.130827

Kim, K.-H., Yun, S.-T., Mayer, B., Lee, J.-H., Kim, T.-S., & Kim, H.-K. (2015). Quantification of nitrate sources in groundwater using hydrochemical and dual isotopic data combined with a Bayesian mixing model. *Agriculture, Ecosystems & Environment, 199*, 369–381. https://doi.org/10.1016/j.agee.2014.10.014

Kotalik, C. J., Cadmus, P., & Clements, W. H. (2021). Before-After Control-Impact field surveys and novel experimental approaches provide valuable insights for characterizing stream recovery from acid mine drainage. *Science of the Total Environment, 771*, 145419. https://doi.org/10.1016/j.scitotenv.2021.145419

Li, J., Kawashima, N., Fan, R., Schumann, R. C., Gerson, A. R., & Smart, R. S. (2014). Method for distinctive estimation of stored acidity forms in acid mine wastes. *Environmental Science and Technology, 48*, 11445–11452. https://doi.org/10.1021/es502482m

Li, S., Xu, Z., Wang, H., Wang, J., & Zhang, Q. (2009). Geochemistry of the upper Han River basin, China: 3: Anthropogenic inputs and chemical weathering to the dissolved load. *Chemical Geology, 264*, 89–95. https://doi.org/10.1016/j.chemgeo.2009.02.021

Li, S., & Zhang, Q. (2010). Risk assessment and seasonal variations of dissolved trace elements and heavy metals in the Upper Han River China. *Journal of Hazardous Materials, 181*, 1051–1058. https://doi.org/10.1016/j.jhazmat.2010.05.120

Liu, X., Zuo, R., Wang, J., He, Z., & Li, Q. (2021). Advances in researches on ammonia, nitrite and nitrate on migration and transformation in the groundwater level fluctuation zone. *Hydrogeology & Engineering Geology, 48*, 27–36. https://doi.org/10.16030/j.cnki.issn.1000-3665.202007033

Liu, Q., Chen, B., Haderlein, S., Gopalakrishnan, G., & Zhou, Y. (2018). Characteristics and environmental response of secondary minerals in AMD from Dabaoshan Mine, South China. *Ecotoxicology and Environmental Safety, 155*, 50–58. https://doi.org/10.1016/j.ecoenv.2018.02.017

Liu, Y., Wei, L., Wu, Q., Luo, D., Xiao, T., Wu, Q., Huang, X., Liu, J., Wang, J., & Zhang, P. (2023). Impact of acid mine drainage on groundwater hydrogeochemistry at a pyrite mine (South China): A study using stable isotopes and multivariate statistical analyses. *Environmental Geochemistry and Health, 45*, 771–785. https://doi.org/10.1007/s10653-022-01242-8

López, J., Reig, M., Gibert, O., & Cortina, J. L. (2019). Recovery of sulphuric acid and added value metals (Zn, Cu and rare earths) from acidic mine waters using nanofiltration membranes. *Separation and Purification Technology, 212*, 180–190. https://doi.org/10.1016/j.seppur.2018.11.022

Mayo, A. L., Petersen, E. C., & Kravits, C. (2000). Chemical evolution of coal mine drainage in a non-acid producing environment, Wasatch Plateau, Utah USA. *Journal of Hydrology, 236*, 1–16. https://doi.org/10.1016/S0022-1694(00)00277-8

McGregor, R. G., Blowes, D. W., Jambor, J. L., & Robertson, W. D. (1998). Mobilization and attenuation of heavy metals within a nickel mine tailings impoundment near Sudbury, Ontario. *Canada. Environmental Geology, 36*, 305–319. https://doi.org/10.1007/s002540050346

Moreno-González, R., Macías, F., Olías, M., & Ruiz, C. C. (2022). Temporal evolution of acid mine drainage (AMD) leachates from the abandoned tharsis mine (Iberian Pyrite Belt, Spain). *Environmental Pollution, 295*, 118697. https://doi.org/10.1016/j.envpol.2021.118697

Naidu, G., Ryu, S., Thiruvenkatachari, R., Choi, Y., Jeong, S., & Vigneswaran, S. (2019). A critical review on remediation, reuse, and resource recovery from acid mine drainage. *Environmental Pollution, 247*, 1110–1124. https://doi.org/10.1016/j.envpol.2019.01.085

Newman, C. P., Walton-Day, K., Runkel, R. L., & Wilkin, R. T. (2023). Mechanisms of water-rock interaction and implications for remediating flooded mine workings elucidated from environmental tracers, stable isotopes, and rare earth elements. *Applied Geochemistry, 157*, 105769. https://doi.org/10.1016/j.apgeochem.2023.105769

Nordstrom D., Alpers C. (1999). Geochemistry of acid mine waters, *The Environmental Geochemistry of Mineral Deposits*, pp. 133–160

Parkhurst, D. L., & Appelo, C. (1999). User's guide to PHREEQC (Version 2): A computer program for speciation, batch-reaction, one-dimensional transport, and inverse geochemical calculations. *Water-Resources Investigations Report, 99*, 312.

Qian, G., Fan, R., Short, M. D., Schumann, R. C., Li, J., Li, Y., Smart, R. S. C., & Gerson, A. R. (2019). Evaluation of the rate of dissolution of secondary sulfate minerals for effective acid and metalliferous drainage mitigation. *Chemical Geology, 504*, 14–27. https://doi.org/10.1016/j.chemgeo.2018.12.003

Sáinz, A., Grande, J. A., & de la Torre, M. L. (2003). Analysis of the impact of local corrective measures on the input of contaminants from the Odiel River to the Ría of Huelva (Spain). *Water, Air, and Soil Pollution, 144*, 375–389. https://doi.org/10.1023/A:1022905502320

Sánchez, E. J., López, P. E., Santofimia, E., Aduvire, O., Reyes, J., & Barettino, D. (2005). Acid mine drainage in the Iberian Pyrite Belt (Odiel river watershed, Huelva, SW Spain): Geochemistry, mineralogy and environmental implications. *Applied Geochemistry, 20*, 1320–1356. https://doi.org/10.1016/j.apgeochem.2005.01.011

Santisteban, M., Luís, A., Grande, J., Aroba, J., Dávila, J., Sarmiento, A., Garrido, J. C., Cordoba, F., & Rodriguez, A. (2022). Hydrochemical characterization of an acid mine effluent from Concepcion mine using classical statistic and fuzzy logic techniques. *Minerals, 12*, 464. https://doi.org/10.3390/min12040464

Sarmiento, A. M., Nieto, J. M., Olías, M., & Cánovas, C. R. (2009). Hydrochemical characteristics and seasonal influence on the pollution by acid mine drainage in the Odiel river Basin (SW Spain). *Applied Geochemistry, 24*, 697–714. https://doi.org/10.1016/j.apgeochem.2008.12.025

Schmidt, M. J., Pankavich, S. D., Navarre-Sitchler, A., Engdahl, N. B., Bolster, D., & Benson, D. A. (2020). Reactive particle-tracking solutions to a benchmark problem on heavy metal cycling in lake sediments. *Journal of Contaminant Hydrology, 234*, 103642. https://doi.org/10.1016/j.jconhyd.2020.103642

Schoepfer, V. A., & Burton, E. D. (2021). Schwertmannite: A review of its occurrence, formation, structure, stability and interactions with oxyanions. *Earth-Science Reviews*. https://doi.org/10.1016/j.earscirev.2021.103811

Servida, D., Grieco, G., & De Capitani, L. (2009). Geochemical hazard evaluation of sulphide-rich iron mines: The Rio Marina district (Elba Island, Italy). *Journal of Geochemical Exploration, 100*, 75–89. https://doi.org/10.1016/j.gexplo.2008.03.005

Sharif, M. U., Davis, R. K., Steele, K. F., Kim, B., Kresse, T. M., & Fazio, J. A. (2008). Inverse geochemical modeling of groundwater evolution with emphasis on arsenic in the Mississippi River Valley alluvial aquifer, Arkansas (USA). *Journal of Hydrology, 350*, 41–55. https://doi.org/10.1016/j.jhydrol.2007.11.027

Shum, M., & Lavkulich, L. (1999). Speciation and solubility relationships of Al, Cu and Fe in solutions associated with sulfuric acid leached mine waste rock. *Environmental Geology, 38*, 59–68. https://doi.org/10.1007/s002540050401

Simate, G. S., & Ndlovu, S. (2014). Acid mine drainage: Challenges and opportunities. *Journal of Environmental Chemical Engineering, 2*, 1785–1803. https://doi.org/10.1016/j.jece.2014.07.021

Soltani, N., Moore, F., Keshavarzi, B., & Sharifi, R. (2014). Geochemistry of trace metals and rare earth elements in stream water, stream sediments and acid mine drainage from Darrehzar Copper Mine, Kerman. *Iran. Water Qual. Exposure Health, 6*, 97–114. https://doi.org/10.1007/s12403-014-0114-x

Tomiyama, S., Igarashi, T., Tabelin, C. B., Tangviroon, P., & Ii, H. (2020). Modeling of the groundwater flow system in excavated areas of an abandoned mine. *Journal of Contaminant Hydrology, 230*, 103617. https://doi.org/10.1016/j.jconhyd.2020.103617

Torres-Martínez, J. A., Mora, A., Mahlknecht, J., Daesslé, L. W., Cervantes-Avilés, P. A., & Ledesma-Ruiz, R. (2021). Estimation of nitrate pollution sources and transformations in groundwater of an intensive livestock-agricultural area (Comarca Lagunera), combining major ions, stable isotopes and MixSIAR model. *Environmental Pollution, 269*, 115445. https://doi.org/10.1016/j.envpol.2020.115445

Tu, Z., Wu, Q., He, H., Zhou, S., Liu, J., He, H., Liu, C., Dang, Z., & Reinfelder, J. R. (2022). Reduction of acid mine drainage by passivation of pyrite surfaces: A review. *Science of the Total Environmen*. https://doi.org/10.1016/j.scitotenv.2022.155116

Wu, Y., Shen, Z., & Zhong, Z. (2006). Chemical origin of acid mine drainage and its computer simulation with Phreeqc—A case study of Zibo coal mining district. *Chinese Journal of Geochemistry, 25*, 26–26. https://doi.org/10.1007/BF02839783

Xiying, G., Binghui, C., Lina, C., Wen, L., & Yao, Z. (2020). The relationship among iron ion, secondary mineral assemblage and heavy metals distribution in the acid mine drainage (AMD) at Dabaoshan mine, Guangdong province. *Acta Scientiarum Naturalium Universitatis Sunyatseni, 59*, 12. https://doi.org/10.13471/j.cnki.acta.snus.2020.03.002

Yang, C., Lu, G., Xie, Y., Guo, L., Chen, M., Ge, L., & Dang, Z. (2021). Sulfate migration and transformation characteristics in paddy soil profile affected by acid mine drainage. *Environmental Research, 200*, 111732. https://doi.org/10.1016/j.envres.2021.111732

Yue, M., Zhao, F. H., & Ren, D. Y. (2006). Simulating experiments to the soluble metals migration of Co, Ni, Zn, Cd, Al, Cr, As and Pb in acid coal-mine drainage. *Acta Scientiae Circumstantiae, 26*, 949–953. https://doi.org/10.13671/j.hjkxxb.2006.06.013

Zhang, Y., Zhang, R., Wu, P., Chen, S., Yang, Y., An, L., Fu, Y., & Zhang, Y. (2022). Adsorption mechanisms and effect factors of As(V) by AMD sludge composite material. *Environmental Science*. https://doi.org/10.13227/j.hjkx.202108230

Zhao, H., Xia, B., Qin, J., & Zhang, J. (2012). Hydrogeochemical and mineralogical characteristics related to heavy metal attenuation in a stream polluted by acid mine drainage: A case study in Dabaoshan Mine. *Chinese Journal of Environmental Science, 24*, 979–989. https://doi.org/10.1016/S1001-0742(11)60868-1